



Hollow lithium manganese oxide nanotubes using MnO₂-carbon nanofiber composites as cathode materials for hybrid capacitors



Dong-Yo Sin, Bon-Ryul Koo, Hyo-Jin Ahn*

Department of Materials Science and Engineering, Seoul National University of Science and Technology, Seoul 139-743, Republic of Korea

ARTICLE INFO

Article history:

Received 29 April 2016

Received in revised form

2 November 2016

Accepted 19 November 2016

Available online 22 November 2016

Keywords:

Lithium manganese oxide

Hollow structure

Electrospinning

Solid-state reaction

Electrochemical capacitor

ABSTRACT

To improve the electrochemical performance of hybrid capacitors, hollow lithium manganese oxide (LiMn₂O₄, LMO) nanotubes (NTs) as cathode materials were synthesized by a solid-state reaction, using MnO₂ coated on a porous carbon nanofiber (PCNF) templates. To determine the optimum shell thickness of hollow LMO, the time of MnO₂ coating on PCNF was adjusted to 10, 30, and 60 min. Among these, hollow LMO NTs, which were synthesized by 30-min coating with MnO₂ on the PCNFs, have superior performance. They exhibited an excellent reversible capacity (~72.8 mAh g⁻¹) at 1 C, capacity retention of ~98.4% after 100 cycles, and an excellent high-rate capability. This superior performance can be explained by the hollow structure giving a reduced diffusion distance for Li-ions, the networked structure of one-dimensional NTs allowing fast charge transfer, and the achievement of the optimal stoichiometric ratio of the LMO phase.

© 2016 Elsevier B.V. All rights reserved.

1. Introduction

Hybrid capacitors (HCs) have received considerable interest for use in various applications such as portable electronics, electric cars, and generators [1–3]. One type of HC, lithium-ion capacitors (LICs), combining the advantages of lithium-ion batteries (LIBs) and electric double-layer capacitors (EDLCs), have recently been investigated for applications requiring high energy density and high power density simultaneously [4–6]. LICs are composed of an anode, a cathode, a separator, and an electrolyte. Among these, the choice of cathode material, for example LiCoO₂ (LCO), LiNiO₂ (LNO), or LiMn₂O₄ (LMO), directly affects the electrochemical performance of LICs [7,8]. LMO is particularly attractive as a cathode material for various reasons including its high theoretical capacity (~148 mAh g⁻¹), high power density, and low cost [9–11]. However, it suffers from capacity fading during cycles and a poor rate capability due to structural degradation. From a morphology perspective, one-dimensional (1-D) nanostructures such as nanowires, nanorods, and nanobelts have recently been receiving considerable attention because they possess unique structures with relatively large surface-to-aspect ratios and demonstrate efficient charge transport pathways [12]. The preparation of LMO 1-D nanostructures, has been attempted by various synthetic methods including a

precipitation method, a microemulsion method, and a solid-state method. For example, Meng et al. synthesized 1-D LMO nanowires using a precipitation method, which exhibited a reversible capacity of ~63 mAh g⁻¹ and capacity retention of ~70.4% after 50 cycles at 0.2 C [13]. Cheng et al. fabricated LMO nanorods by a microemulsion-based method and a solid-state reaction, which showed the reversible capacity of ~57 mAh g⁻¹ and capacity retention of ~86.0% after 500 cycles at 10 C [14]. Despite these efforts, the development of hollow LMO nanostructures for hybrid capacitors has not yet been reported. This hollow nanostructure has the unique properties of the reduced the diffusion length of Li-ions and alleviation of volume expansion, which can cause the improvement of electrochemical performances for hybrid capacitors [15,16]. In this study, we synthesized hollow LMO NTs using MnO₂ coated on a porous carbon nanofiber (PCNF) template by means of electrospinning, direct redox reaction, and a solid-state reaction. We used these to demonstrate the correlation between their structural properties and electrochemical performance as cathode materials.

2. Experiments

2.1. Synthesis of hollow lithium manganese oxide (LiMn₂O₄, LMO) nanotubes (NTs)

Hollow LiMn₂O₄ (LMO) nanotubes (NTs) were synthesized by a

* Corresponding author.

E-mail address: hjahn@seoultech.ac.kr (H.-J. Ahn).

solid-state reaction using MnO₂-coated porous carbon nanofibers (PCNFs) as a template. The MnO₂-coated PCNF templates, which are crucial for formation of the desired hollow structures, were prepared by a combination of electrospinning and direct redox reaction. The PCNFs were obtained using electrospinning. Firstly, 10 wt% polyacrylonitrile (PAN, M_w = 150,000 g mol⁻¹, Aldrich) and 0.5 wt% poly (styrene-co-acrylonitrile) (SAN, M_w = 165,000 g mol⁻¹, Aldrich) were dissolved in *N,N*-dimethylformamide (DMF, Aldrich). Subsequently, the prepared solution was loaded into a syringe equipped with a 23-gauge needle. The feeding rate and the distance between the needle and collector were fixed at ~0.03 mL h⁻¹ and ~15 cm, respectively. To collect the spun nanofibers, a working voltage was applied of ~13 kV using a DC power supply (Powertron. Co. Ltd, Korea). The nanofibers were then stabilized at 280 °C for 2 h in air before carbonizing at 800 °C for 2 h in an N₂ atmosphere. The MnO₂ coating was added by a direct redox reaction, performed by mixing two solutions. One of the PCNFs dispersed in 2.0 M H₂SO₄ and the other of KMnO₄ dissolved in DI-water. The mixed solutions were reacted at 80 °C, the reaction time was varied to 10, 30, or 60 min to obtain different MnO₂ layer thicknesses on the PCNFs. Finally, the MnO₂ coated PCNFs were washed using DI-water and dried at 80 °C for 10 h. To synthesize the hollow LMO NTs, the MnO₂ coated PCNFs were mixed with LiOH·H₂O in a molar ratio of 2:1. This mixture was heated at 480 °C for 3 h and then 750 °C for 10 h in air giving hollow LMO NTs. For comparison, some LMO nanoparticles were fabricated using the above-mentioned method, but without the PCNFs template. Thus, we obtained LMO particles and three types of hollow LMO NTs formed by coating PCNFs with MnO₂ for 10, 30, and 60 min (referred to herein as P-LMO, H-LMO10, H-LMO30, and H-LMO60, respectively).

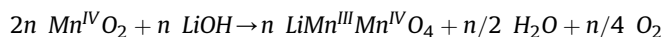
2.2. Characterization

The morphological properties of the samples were determined by field emission-scanning electron microscopy (FESEM; Hitachi S-4800) and transmission electron microscopy (TEM; JEOL, 2100F, KBSI Suncheon Center). The crystal structures and chemical bonding states were determined by X-ray diffraction (XRD, Rigaku D/MAX2500V) with Cu K α radiation in the angular range of 10°–90° with a step size of 0.02° and X-ray photoelectron spectroscopy (XPS, ESCALAB250) with an Al K α X-ray source under a base pressure of 267 nPa, respectively. The electrochemical performance of the samples was investigated using Li coin cells (CR2032, Hohsen Corporation). The Li coin cells were composed of Li metal foil (Honjo Chemical, 99.8%) as the anode, the prepared samples as the cathode, a porous polypropylene membrane (Celgard 2400) as the separator, and a 1.0 M LiPF₆ solution in a mixture of ethylene carbonate and dimethyl carbonate (1:1) as the electrolyte. To fabricate the cathodes, slurries of the prepared samples

(70 wt%) as active material, ketjen black (10 wt%, Alfa Aesar) as a conducting material, and poly (vinylidene difluoride) (20 wt%) as a binder in *N*-methyl-2-pyrrolidinone solvent (NMP, Aldrich), were coated onto an Al foil substrate (aluminum foil, 15 μ m). This was then dried at 100 °C for 12 h. The Li coin cells were assembled in a high-purity argon-filled glove box (<5 ppm, H₂O and O₂). The electrochemical impedance spectroscopy (EIS) measurements were performed in fresh cells over a frequency range of 100 kHz to 10 mHz at an AC signal strength of 5 mV. The galvanostatic charge-discharge measurements were performed using a WMPG 3000 battery cycler system (WonATech Corp., Korea) over a potential range of 3.3–4.3 V (versus Li/Li⁺) at 25 °C. The cycle number dependence was measured up to 100 cycles at a current density of 1 C (120 mA g⁻¹). The rate performance of all the samples was investigated at C-rates of 1 C, 3 C, 5 C, 7 C, and 10 C before testing again at 1 C.

3. Results and discussion

Fig. 1 shows a schematic of the synthesis of hollow LMO NTs. As shown in Fig. 1a, the PCNFs were synthesized by electrospinning using a mixed solution of PAN and SAN polymers. The resultant PCNFs have micro-pores resulting from decomposition of the added SAN polymers during stabilization, which gives the enhanced surface area required to form a uniform MnO₂ shell [17]. Then the MnO₂ coating of the above-mentioned PCNFs was added by direct redox reaction (Fig. 1b). The MnO₂ coating on the PCNFs was used as the main matrix to form the LMO phase by a solid-state reaction using LiOH·H₂O, as shown by the following equation [18].



Combustion of the PCNFs generates the hollow core of the nanostructures, resulting in the formation of hollow LMO NTs (Fig. 1c). Thus, we successfully synthesized hollow LMO NTs by a three step process consisting of electrospinning, direct redox reaction, and solid-state reaction.

Fig. 2a–d shows the FESEM images of P-LMO, H-LMO10, H-LMO30, and H-LMO60. The morphology of P-LMO shows diameters in the range of ~0.83–~1.77 μ m resulting from irregular aggregation. On the other hand, H-LMO10, H-LMO30, and H-LMO60 are observed as hollow nanotubes with holes ~210.3–231.5 nm in diameter. The formation of this nanostructure is induced by the combustion of the PCNFs during the solid-state reaction. The diameters and shell thicknesses of the hollow NTs are observed to be ~443.9–526.4 nm and ~77.0–113.3 nm for H-LMO10, ~474.4–526.4 nm and ~116.4–157.3 nm for H-LMO30, and ~513.2–583.5 nm and ~156.2–203.3 nm for H-LMO60, respectively. Their diameters and shell thicknesses increase with the thickness of

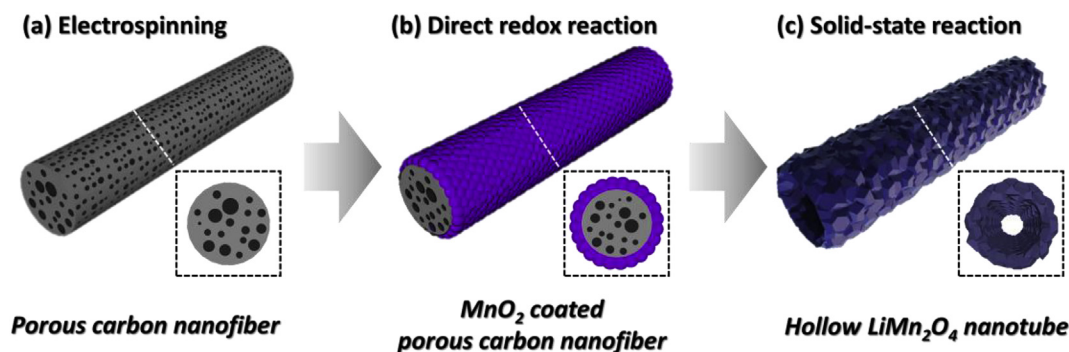


Fig. 1. A schematic illustration of process steps to fabricate the hollow LMO nanotubes.

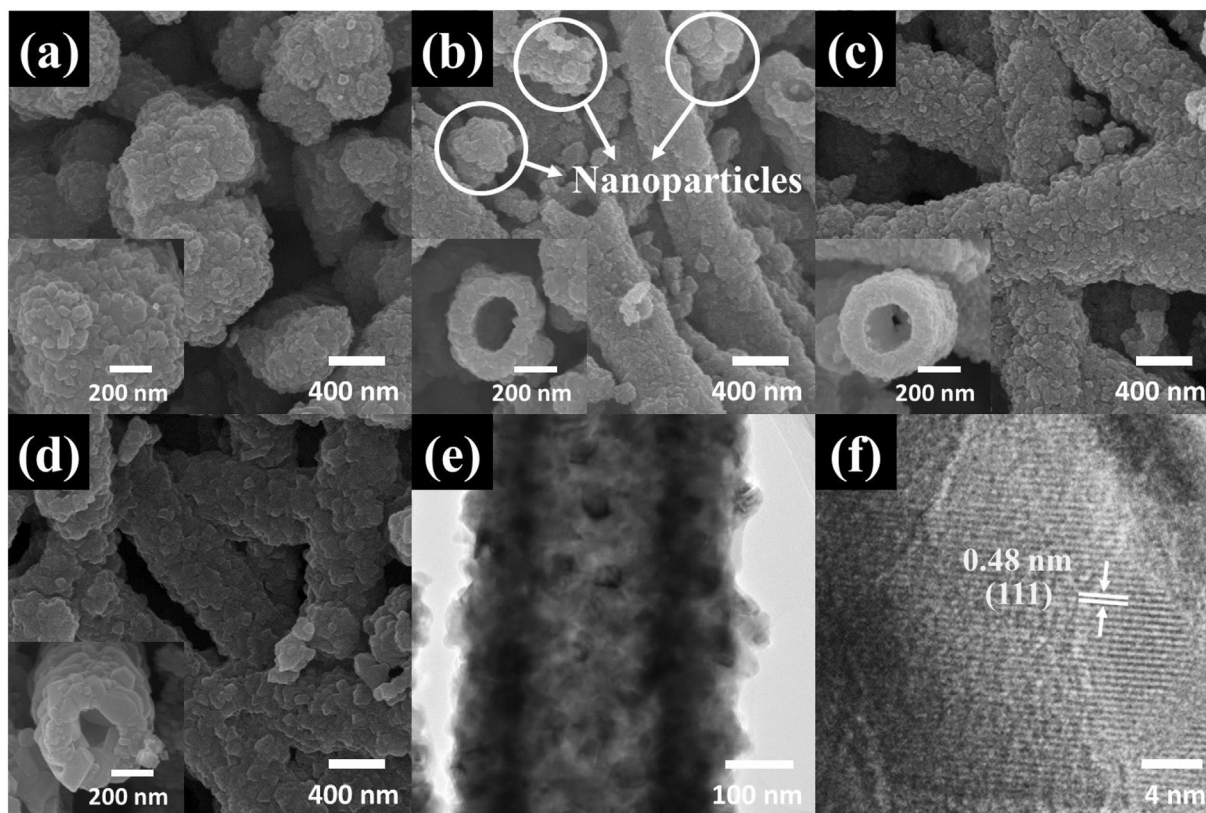


Fig. 2. FESEM images [(a)–(d)] of P-LMO, H-LMO10, H-LMO30, and H-LMO60, and TEM images [(e)–(f)] of H-LMO30.

the MnO_2 in shell region, which can be controlled by the reaction time allowed for the direct redox reaction. The H-LMO10 sample shows hollow NTs as well as nanoparticles owing to partial disruption of the thin MnO_2 shell formed in the solid-state reaction. On destruction of the LMO shell the advantage of the network structure of NTs, that can provide the fast charge transfer, is lost [19]. In contrast, H-LMO30 and H-LMO60 contain solely the desired hollow NTs, which can shorten the diffusion distance of the Li-ions and aid fast charge transfer in the electrodes. Fig. 2e–f shows TEM images of H-LMO30. In the low magnification image, H-LMO30 consists of a core area of gray contrast and an edge area of dark contrast, this is indicative of a hollow structure. The high magnification image of H-LMO30 indicates that the individual grains are clearly crystallized. In addition, an interlayer spacing of ~ 0.48 nm is indicated from the (111) plane of the spinel LMO structure as shown in Fig. 2f [20].

Fig. 3a shows XRD data for P-LMO, H-LMO10, H-LMO30, and H-LMO60. All of the samples show sharp, intense peaks, which indicate the main characteristic diffraction peaks at 18.6° , 36.1° , 43.9° , and 63.8° . Each of the peaks corresponds to the (111), (311), (400), and (440) planes of the spinel LMO with the space group of $\text{Fd-}3\text{m}$ (JCPDS card No. 035-0782) [21]. However, H-LMO60 shows diffraction peaks for both spinel LMO and Mn_3O_4 phases. The Mn_3O_4 phase is formed by an excessive amount of MnO_2 when the redox reaction is performed for 60 min. The excessive amount of MnO_2 does not react with the added Li source. The MnO_2 is partially transformed to Mn_3O_4 by combining with oxygen during the solid-state reaction [22]. To investigate the chemical binding states of H-LMO10, H-LMO30, and H-LMO60, XPS analysis was performed as shown in Fig. 3b–d. The Mn 2p XPS spectral peaks of H-LMO10, H-LMO30, and H-LMO60 show two different signals at ~ 642.4 eV and ~ 654.1 eV, corresponding to Mn $2\text{p}_{3/2}$ and Mn $2\text{p}_{1/2}$, respectively. In

addition, the Mn $2\text{p}_{3/2}$ is separated into two peaks corresponding to the Mn(III) and Mn(IV) states [23]. Formally, LiMn_2O_4 is referred to as $\text{LiMn}^{\text{III}}\text{Mn}^{\text{IV}}\text{O}_4$. The Mn(III) and Mn(IV) states exist simultaneously in a 1:1 ratio due to their stoichiometric ratio in LMO. Thus, the Mn(III) content of all of the samples is calculated by the following equation [24].

$$C_x = (A_i/\text{ASF}_i) / \sum (A_j/\text{ASF}_j)$$

In this equation A_i is the area under the i th peak and ASF_i is atomic sensitivity factor. The Mn(III) content of the samples was calculated to be $\sim 49.9\%$ for H-LMO10, $\sim 50.3\%$ for H-LMO30, and $\sim 56.9\%$ for H-LMO60, respectively. This result confirms that H-LMO10 and H-LMO30 form a perfect LMO phase. The increased Mn(III) present in H-LMO60 results from the formation of a Mn_3O_4 phase [25]. Thus, based on the FESEM, TEM, XRD, and XPS data, we successfully synthesized hollow LMO NTs.

Fig. 4a shows the Nyquist plots of all the samples in the frequency range 100 kHz to 10 mHz. The charge transfer impedance (R_{ct}) at the electrode/electrolyte interface shows as a semicircle in the medium-frequency range. The diffusion of Li-ions in the electrodes shows an inclined line, which is the Warburg impedance [26]. H-LMO30 shows a much smaller semicircle, with the lowest Warburg impedance of the compared to other samples. This result for H-LMO30 indicates that it has an excellent electrical conductivity owing to a reduced diffusion distance of Li-ions arising from its optimum hollow structure and fast charge transfer by the networked structure of NTs.

Fig. 4b shows the charge-discharge profiles of all the samples obtained after the 1st cycle. Two plateaus at ~ 3.94 and ~ 4.11 V are observed in all of the samples, indicating the lithium ion insertion and extraction reactions. The reaction has been described by

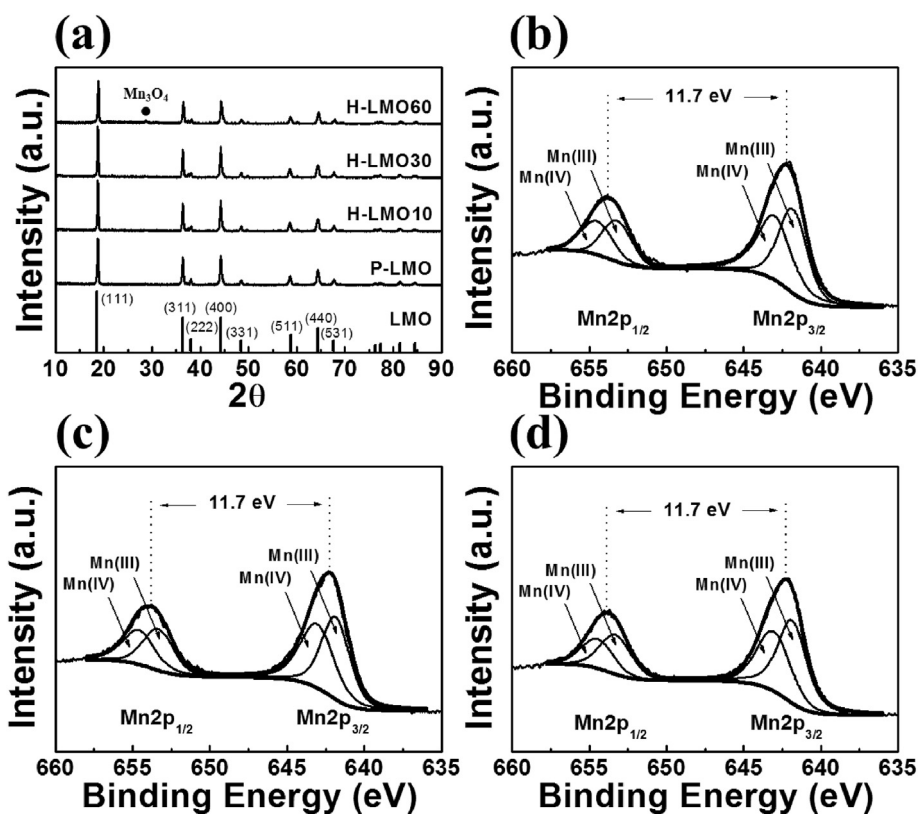


Fig. 3. (a) XRD plots of P-LMO, H-LMO10, H-LMO30, and H-LMO60. XPS spectra [(b)–(d)] of H-LMO10, H-LMO30, and H-LMO60.

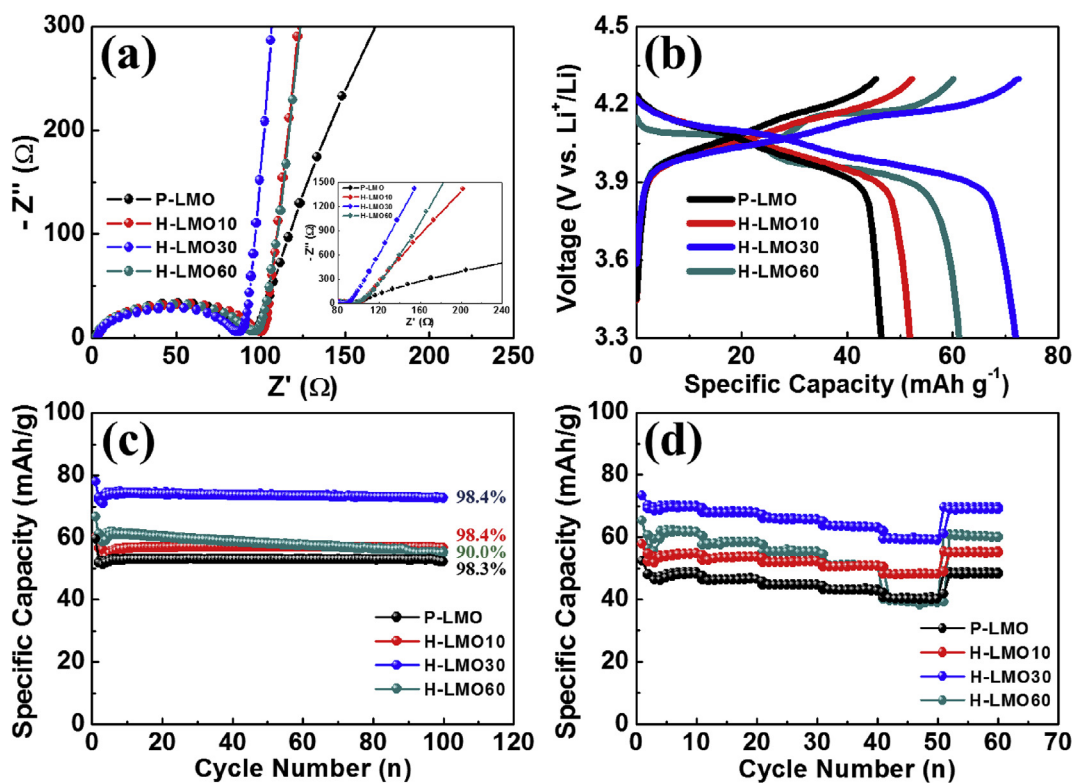
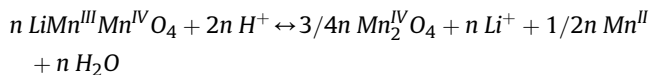


Fig. 4. (a) Nyquist plots of the P-LMO, H-LMO10, H-LMO30, and H-LMO60 in the frequency range of 100 kHz to 10 mHz before the charge-discharge test. (b) Galvanostatic charge-discharge curves of cells fabricated with P-LMO, H-LMO10, H-LMO30, and H-LMO60. (c) The cycling number dependence of the P-LMO, H-LMO10, H-LMO30, and H-LMO60 up to 100th cycles at 1 C. (d) The rate performance of all the samples obtained from C-rates of 1 C, 3 C, 5 C, 7 C, 10 C, and 1 C.

Hunter, by the following equation [17].



The charge and discharge capacities are observed as ~46.4 and ~45.5 mAh g⁻¹ for P-LMO, ~51.9 and ~51.8 mAh g⁻¹ for H-LMO10, ~73.7 and ~73.5 mAh g⁻¹ for H-LMO30, and ~61.2 and ~60.1 mAh g⁻¹ for H-LMO60, respectively. Among them, H-LMO30 exhibited the highest reversible capacity owing to its optimum hollow structure and its networked structure of NTs. These respectively reduce the diffusion distance for Li-ions and aid in fast charge transfer.

Fig. 4c shows the cycle number dependence of the charge-discharge capacities of all the samples. Reversible capacities of P-LMO, H-LMO10, H-LMO30, and H-LMO60 were ~52.2 mAh g⁻¹, ~55.1 mAh g⁻¹, ~72.8 mAh g⁻¹, and ~54.9 mAh g⁻¹ after 100 cycles. In addition, their capacity retentions are observed as ~98.3%, ~98.4%, ~98.4%, and ~90.0%, respectively. P-LMO shows the lowest reversible capacity owing to the long diffusion distance of Li-ions caused by the large size of the LMO aggregates. This is consistent with the Warburg impedance determined from the EIS data. In the case of H-LMO10, a low reversible capacity is observed due to the coexistence of NTs and nanoparticles, which causes the observed reduction of charge transfer. H-LMO30 exhibits good reversible capacity and excellent capacity retention, because it has both the shortest diffusion distance for Li-ions due to its optimized hollow structure and the fastest charge transfer from its networked structure of NTs. Furthermore, with H-LMO60, the reversible capacities decrease continuously up to 100 cycles owing to the presence of Mn₃O₄, which can allow dissolution of Mn³⁺ resulting in volume expansion. Thus, H-LMO60 exhibited poor reversible capacity compared to H-LMO30 in spite of the presence of a hollow nanostructure.

Fig. 4d shows the rate performance of all the samples obtained from various C-rates of 1 C, 3 C, 5 C, 7 C, 10 C, and 1 C again. The reversible capacities of all the samples recovered to ~99% of the original value, when the 10 C rate was decreased back to 1 C. In particular, H-LMO30 maintained the best high-rate capability of compared to all the samples. Its reversible capacity decreases from ~70.3 to ~59.8 mAh g⁻¹ when increasing from 1 C to 10 C, but returns to ~69.6 mAh g⁻¹ on reduction back to 1 C. This result is due to their optimum hollow structure and the networked structure of NTs. However, H-LMO60 exhibits a rapid drop of the reversible capacity at 10 C owing to existence of Mn₃O₄. Therefore, the improved electrochemical performance of H-LMO30 as cathode materials such as its superior reversible capacity, capacity retention, and high-rate capability, are owed to a combination of factors. Their optimum hollow structure giving a reduced diffusion distance for Li-ions, the networked structure of NTs allowing fast charge transfer, and the appropriate stoichiometric ratio of ions in the LMO phase improving reversible capacity particularly. Thus, hollow LMO NTs, which are synthesized by a solid-state reaction using a MnO₂ coated PCNF template, should be considered as potential candidates for use as cathode materials in hybrid capacitors.

4. Conclusions

Hollow LMO NTs were successfully synthesized by a solid-state

reaction using MnO₂ coated on PCNF templates. The shell thickness of the hollow LMO NTs was controlled by varying the thickness of the MnO₂ shell. This was achieved by adjusting the redox reaction time to 10, 30, or 60 min. Among the materials, hollow LMO NTs synthesized by coating the PCNFs with MnO₂ for 30 min (H-LMO30) displayed superior performance. They had a good reversible capacity (~72.8 mAh g⁻¹) at 1 C, excellent capacity retention (~98.4%) after 100 cycles, and excellent high-rate capability. This enhanced electrochemical performance is due to the reduced diffusion distance of Li-ions owing to the hollow structure, fast charge transfer because of the networked structure of NTs, and the optimum stoichiometric ratio ions in the LMO phase. Thus, hollow LMO NTs which use MnO₂ coated on PCNF templates are promising candidates for use as cathode materials in high-performance hybrid capacitors.

Acknowledgement

This work was supported by the Industrial Fundamental Technology Development Program (10052745, Development of nano-sized(100 nm) manganese ceramic material for high voltage pseudo-capacitor) funded by the Ministry of Trade, Industry and Energy (MOTIE) of Korea.

References

- [1] A. Vlad, N. Singh, J. Rolland, S. Melinte, P.M. Ajayan, J.-F. Gohy, *Sci. Rep.* 4 (2014) 4315.
- [2] H. Zhang, Y. Huang, B. Xu, G. Cao, *Electrochem. Solid State Lett.* 1 (2012) M1–M3.
- [3] Z.K. Ghouri, M.S. Akhtar, A. Zahoor, N.A. Barakat, W. Han, M. Park, B. Pant, P.S. Saud, C.H. Lee, H.Y. Kim, *J. Alloys Compd.* 642 (2015) 210–215.
- [4] G.-H. An, B.-R. Koo, H.-J. Ahn, *Phys. Chem. Chem. Phys.* 18 (2016) 6587–6594.
- [5] X. Liu, H.-G. Jung, S.-O. Kim, H.-S. Choi, S. Lee, J.H. Moon, J.K. Lee, *Sci. Rep.* 3 (2013) 3183.
- [6] J.-B. Lee, S.-Y. Jeong, W.-J. Moon, T.-Y. Seong, H.-J. Ahn, *J. Alloys Compd.* 509 (2011) 4336–4340.
- [7] M. Okubo, E. Hosono, J. Kim, M. Enomoto, N. Kojima, T. Kudo, H. Zhou, I. Honma, *J. Am. Chem. Soc.* 129 (2007) 7444–7452.
- [8] M.Y. Song, R. Lee, *J. Power Sources* 111 (2002) 97.
- [9] C.M. Julien, M. Massot, *Mater. Sci. Eng. B* 100 (2003) 69.
- [10] G. Xu, Z. Liu, C. Zhang, G. Cui, L. Chen, *J. Mater. Chem. A* 3 (2015) 4092.
- [11] D. Guo, X. Wei, Z. Chang, H. Tang, B. Li, E. Shangguan, K. Chang, X.-Z. Yuan, H. Wang, *J. Alloys Compd.* 632 (2015) 222–228.
- [12] D.K. Kim, P. Murallidharan, H.-W. Lee, R. Ruffo, Y. Yang, C.K. Chan, H. Peng, R.A. Huggins, Y. Cui, *Nano Lett.* 8 (2008) 3948.
- [13] Y. Meng, X. Liu, L. Liu, B. Li, X. Zhao, L. Feng, Y. Wang, X. Wang, *Chem. Res. Chin. Univ.* 31 (2015) 820.
- [14] F. Cheng, H. Wang, Z. Zhu, Y. Wang, T. Zhang, Z. Tao, J. Chen, *Energy Environ. Sci.* 4 (2011) 3668.
- [15] G. Jian, Y. Xu, L.-C. Lai, C. Wang, *J. Mater. Chem. A* 2 (2014) 4627.
- [16] Y. Wu, Z. Wen, H. Feng, J. Li, *Small* 8 (2012) 858.
- [17] B.-S. Lee, S.-B. Son, K.-M. Park, G. Lee, K.H. Oh, S.-H. Lee, W.-R. Yu, *ACS Appl. Mater. Interfaces* 4 (2012) 6702.
- [18] Y. Chen, K. Xie, Y. Pan, C. Zheng, *Solid State Ionics* 181 (2010) 1445.
- [19] J.-Y. Luo, H.-M. Xiong, Y.-Y. Xia, *J. Phys. Chem. C* 112 (2008) 12051.
- [20] Y.-L. Ding, X.-B. Zhao, J. Xie, G.-S. Cao, T.-J. Zhu, H.-M. Yu, C.-Y. Sun, *J. Mater. Chem.* 21 (2011) 9475.
- [21] H.W. Chan, J.G. Duh, S.R. Sheen, *J. Power Sources* 115 (2003) 110.
- [22] J. Cho, M.M. Thackeray, *J. Electrochem. Soc.* 146 (1999) 3577.
- [23] X. Zhao, M.V. Reddy, H. Liu, S. Ramakrishna, G.V. Subba Rao, B.V.R. Chowdari, *RSC Adv.* 2 (2012) 7462.
- [24] A.N. Mansour, C.A. Melendres, *J. Electrochem. Soc.* 142 (1995) 1961.
- [25] A.M.E. Raj, S.G. Victoria, V.B. Jothy, C. Ravidhas, J. Wollschlager, M. Suendorf, M. Neumann, M. Jayachandran, C. Sanjeeviraja, *Appl. Surf. Sci.* 256 (2010) 2920.
- [26] G.-H. An, H.-J. Ahn, *J. Power Sources* 272 (2014) 828.